

Estimation of instrument and noise parameters for inverse problem based on prior diffusion model

Jean-François Giovannelli

Groupe Signal-Image, IMS (Univ. Bordeaux, CNRS, BINP), Talence, France

Abstract — This article addresses the issue of estimating observation parameters (response and error parameters) in inverse problems. The focus is on cases where regularization is introduced in a Bayesian framework and the prior is modeled by a diffusion process. In this context, the issue of posterior sampling is well known to be thorny, and a recent paper [1] proposes a notably simple and effective solution. Consequently, it offers an remarkable additional flexibility when it comes to estimating observation parameters. The proposed strategy enables us to define an optimal estimator for both the observation parameters and the image of interest. Furthermore, the strategy provides a means of quantifying uncertainty. In addition, MCMC algorithms allow for the efficient computation of estimates and properties of posteriors, while offering some guarantees. The paper presents several numerical experiments that clearly confirm the computational efficiency and the quality of both estimates and uncertainties quantification.

Index Terms — Inverse problem, deconvolution, Bayesian, Hyperparameter estimation, Diffusion prior, Gibbs sampler.

I. INTRODUCTION AND PROBLEM FORMULATION

The present paper deals with the resolution of inverse problems [2]–[5] when the observation system is modeled by a linear operator and an additive Gaussian error:

$$\mathbf{y} = \mathbf{H}_\iota \mathbf{x}_0 + \mathbf{e}, \quad (1)$$

where $\mathbf{x}_0 \in \mathbb{R}^P$ collects the unknowns, $\mathbf{y}, \mathbf{e} \in \mathbb{R}^M$ collect the measurements and errors, and $\mathbf{H}_\iota \in \mathbb{R}^P \times \mathbb{R}^M$ characterizes the operator, *e.g.*, a convolution. The vector ι parametrizes the instrument response, typically the width of a Lorentz Point Spread Function (PSF). This is one of the key parameters to be estimated. The second one, denoted η , controls the error pdf. Typically, let us consider an homogeneous white noise with mean m_e and variance v_e . All these parameters are gathered in the vector $\theta = [\iota, \eta]$. These parameters are included among the unknowns and this is a crucial feature of the proposed method to estimate them in addition to the image of interest.

This ability to estimate multiple observation parameters, in addition to the image of interest, is crucial in practice. It is common to have information on instrument parameters or noise levels, for example a nominal value with an associated uncertainty, but it is rare to know them exactly. Furthermore, failing to take into account uncertainties in these parameters leads to erroneous quantification of uncertainties.

This issue has naturally been addressed frequently in the literature and several solutions have been proposed [6]–[12]. They are referred to as auto-adjusted, adaptive, self-tuned, myopic (or blind) or self-calibrated... That said, in the case of priors constructed from the recent diffusion models [13]–[15],

this issue remains difficult and has been little addressed [1]. This difficulty is maybe due to the fact that in this field, the dominant approaches are inherited from ancestral sampling, for which the manipulation of conditional posterior is approximated (they are exact for the prior). For example, to sample the posterior for the images, [16] and [17] rely on approximations that involve the matrix \mathbf{H}_ι itself and this complicates or even makes it impossible in practice to manage the parameters. In contrast, the G-DSP algorithm recently proposed in [1] clearly takes advantage of the Markov structure and conditional independences, which opens up remarkable possibilities for observation parameters estimation.

The paper is organized as follows. Section II introduces the various distributions to model measurements and unknown quantities. Section III describes the posterior sampler. The numerical assessemnt using the MNIST example set is given in Section IV. Finally, Section V proposes a synthesis and includes a few perspectives. Part of the calculations are reported in the Appendix.

II. LIKELIHOOD, PRIOR, POSTERIOR

A. Noise and measurement

The measurements are included *via* the likelihood deduced from the observation model (1) and a model for the error. Here, the latter is described as Gauss with mean m_e and covariance C_e that is to say $\mathcal{N}(\mathbf{e}; m_e, C_e)$. So, the likelihood of the unknowns (\mathbf{x}_0, θ) attached to the measurement \mathbf{y} reads

$$f(\mathbf{y} | \mathbf{x}_0, \theta) = \mathcal{N}(\mathbf{y} ; m_e + \mathbf{H}_\iota \mathbf{x}_0, C_e). \quad (2)$$

Regarding the error, in subsequent developments, we focus on the stationary and white case: the mean and variance are homogeneous and denoted by m_e and v_e respectively and collected in the vector $\eta = [m_e, v_e]$. However, the proposed methodology can easily be generalised to cover more complex situations, and could incorporate correlation parameters, or non-Gaussian noise based on location mixture of Gaussians.

Regarding the vector ι , it collects the parameters of the instrument response. These may include the amplitude and width of the PSF, for example a Lorentzian as considered in the numerical study in Sect. IV. However, the proposed methodology can easily be generalised to more complex PSFs (see, for example [18], [19] and the Moffat PSF).

The vector $\theta = [\iota, \eta]$ collects the unknown observation parameters (instrument and error), the other unknown being the image of interest \mathbf{x}_0 . The aim of the rest of this section is

to incorporate the available knowledge about these unknowns through probability distributions.

- With regard to images, traditional approaches rely, for example, on pixel positivity, pixel correlation, contours or pulses.... Here, we rely on the fact that the image shares a certain resemblance with available examples.
- Regarding the observation parameters, the available information may be an order of magnitude, a nominal value with uncertainty, a minimum / maximum values,...

When the available information is more uncertain, it is referred to as a poorly informative prior.

Among the distributions that allow this information to be taken into account, one seeks to assign a prior so that the posterior (and especially its conditionals) is easy to manipulate and sample. With this in mind, whenever possible, one relies on simple models, such as Gaussian models, and/or on the notion of conjugacy [20].

B. Prior for unknowns

Observation parameter ι — For the instrument parameter, ι , we define a uniform prior between a minimum and a maximum values for each component in line with the knowledge of the physical principles of the instrument. We simply write

$$f_I(\iota) = \mathcal{U}(\iota). \quad (3)$$

In the numerical study of Sect. IV we will consider a Lorentz PSF and ι encode the width.

Noise parameter: offset m_e — Regarding the level of offset in measurements, we consider a situation where a nominal value m_0 and a precision p_0 are available and we define

$$f_M(m_e) = \mathcal{N}(m_e; m_0, p_0^{-1}). \quad (4)$$

In the numerical study of Sect. IV, we will consider the poorly informative case: p_0 is small (and $m_0 = 0$).

Noise parameter: scale γ_e — Regarding γ_e (for notational convenience $\gamma_e = 1/v_e$), a classical choice is a Gamma pdf:

$$f_\Gamma(\gamma) = \mathcal{G}(\gamma; a_0, b_0) \quad (5)$$

This choice makes it easy to consider a nominal value with uncertainty based on the mean a_0/b_0 and the variance a_0/b_0^2 .

Diffusion prior for the images — This prior is described using a diffusion model [13]–[15]: essentially, available examples are transformed into noise, and conversely, new examples are generated by transforming noise realisations. To achieve this, the methodology consists in introducing (i) T latent variables $\mathbf{x}_{1:T}$ (in addition to \mathbf{x}_0) and an extended prior $\pi_{0:T}(\mathbf{x}_{0:T})$ and (ii) two joint pdfs for $\mathbf{x}_{0:T}$: a *forward* denoted $p_{0:T}^+$ and a *backward* denoted $p_{0:T}^-$. For practical efficiency, both are chosen in Markovian form:

$$p_{0:T}^+(\mathbf{x}_{0:T}) = p_0^+(\mathbf{x}_0) \prod_{t=1}^T p_{t|t-1}^+(\mathbf{x}_t | \mathbf{x}_{t-1}) \quad (6)$$

$$p_{0:T}^-(\mathbf{x}_{0:T}) = p_T^-(\mathbf{x}_T) \prod_{t=0}^{T-1} p_{t|t+1}^-(\mathbf{x}_t | \mathbf{x}_{t+1}) \quad (7)$$

which involves two terminal marginal pdfs p_0^+ and p_T^- and two sets of transition pdfs $p_{t|t-1}^+$ and $p_{t|t+1}^-$. Regarding the terminals

$$p_0^+(\mathbf{x}_0) = \pi_0(\mathbf{x}_0) \quad \text{and} \quad p_T^-(\mathbf{x}_T) = \mathcal{N}(\mathbf{x}_T; \mathbf{0}, \mathbf{I})$$

the first is the pdf π_0 of the example set and the second is the pdf of noise (Gaussian, white, zero-mean, unit-variance). With regard to transitions, again for practical efficiency, Gaussians are chosen with the following parameters.

$$p_{t|t-1}^+(\mathbf{x}_t | \mathbf{x}_{t-1}) = \mathcal{N}(\mathbf{x}_t; k_t \mathbf{x}_{t-1}, v_t^+ \mathbf{I}) \quad (8)$$

$$p_{t|t+1}^-(\mathbf{x}_t | \mathbf{x}_{t+1}) = \mathcal{N}(\mathbf{x}_t; \mu_t(\mathbf{x}_{t+1}), v_t^- \mathbf{I}) \quad (9)$$

The function $\mu_t(\mathbf{x})$ is described by a neural network $\mu_t^\theta(\mathbf{x})$, with parameter θ and has two inputs: the image \mathbf{x} and the time t . Replacing μ_t by μ_t^θ in (9), and substituting in (7), yields $p_{0:T}^{\theta, \theta}$. The learning stage adjusts θ to minimise the Kullback distance between the forward $p_{0:T}^+$ and the parametrized backward $p_{0:T}^{\theta, \theta}$ pdfs while ensuring that the marginal pdfs for \mathbf{x}_0 and \mathbf{x}_T are

$$\pi_0 = p_0^+ \simeq p_T^- \quad \text{and} \quad \mathcal{N} = p_T^- \simeq p_T^+$$

i.e., that of the example set and the noise. It suffices then to report the adjusted value of θ in $p_{0:T}^{\theta, \theta}$ to obtain an adjusted joint backward pdf (7). Therefore, based on the latter, it is easy to sample the prior for $\mathbf{x}_{0:T}$, starting from $t = T$ down to $t = 0$ and it is referred to as *ancestral sampling*.

C. Full posterior

We can then construct the joint pdf and the posterior. The latter is based on the likelihood (2) and the priors for the parameters (3), (4), (5), and the joint prior for the images (6)–(7). Its construction relies on conditional independences encoded in the hierarchical model given in Fig. 1.

$$\begin{aligned} \pi_{0:T}(\mathbf{x}_{0:T}, \theta | \mathbf{y}) \propto & \gamma_e^{P/2} \exp -\gamma_e \|(\mathbf{y} - m_e) - \mathbf{H}_e \mathbf{x}_0\|^2 / 2 \\ & \gamma_e^{a_0-1} \exp [-b_0 \gamma_e] \mathbb{1}_{+}(\gamma_e) \\ & \exp [-p_0 (m_e - m_0)^2 / 2] \\ & \mathcal{U}(\iota) \\ & \pi_{0:T}(\mathbf{x}_{0:T}) \end{aligned} \quad (10)$$

Due to the intricate nature of this pdf, it is not possible to compute the estimations and uncertainties directly. To this end, an MCMC sampler is used, as shown below.

III. PROPOSED SAMPLER: A GIBBS SCHEME

To explore the posterior, we resort to a Gibbs loop that splits the global sampling problem in easier sub-problems. More precisely, the conditional posterior of each unknown is sequentially sampled under its conditional density, in an iterative way. The samples form a Markov chain whose distribution converges to the posterior [20], [21].

For each unknown, the conditional pdf given the other unknowns is needed. Each one is proportional to the full posterior (10) and hence it only involves the factors including the considered unknown. Given the hierarchy in Fig. 1,

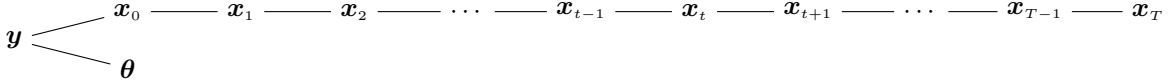


Fig. 1. Hierarchy — \mathbf{x}_0 is the image of interest, $\mathbf{x}_{1:T}$ are the latent images and \mathbf{y} is the measured image (blurred and noisy version of the true \mathbf{x}_0). θ contains the parameters of the observation (response and error), and its estimation is the core of the article. This graph already shows that if we know how to sample the \mathbf{x}_t properly including the conditional independencies encoded by this hierarchy, the difficulty of sampling θ is greatly alleviated.

numerous simplifications arise, which both facilitates the theoretical calculations and reduces the computational load. The conditional posteriors are now given. For notational simplicity $\bar{\mathbf{y}} = \mathbf{y} - m_e$.

A. Image

This section describes the sampling of the extended image $\mathbf{x}_{0:T}$. Up to factor, the pdf writes

$$\exp \left[-\frac{1}{2} \gamma_e \|\bar{\mathbf{y}} - \mathbf{H}_\iota \mathbf{x}_0\|^2 \right] \pi(\mathbf{x}_{0:T})$$

We resort to G-DPS (Gibbs-Diffusion Posterior Sampling) presented in [1]. It itself includes a block-Gibbs sampler: it samples each \mathbf{x}_t in turn under its conditional pdf $\pi_{t|\star}(\mathbf{x}_t | \mathbf{y}, \theta, \mathbf{x}_{t|\star})$ where $(t|\star)$ is the set of times from 0 to T except t itself. The original idea of [1] is to play with both forward and backward pdfs. More specifically, the sampling is based on the posterior attached to the

- forward $\pi_{0:T}^+(\mathbf{x}_{0:T} | \mathbf{y}, \theta)$ for the latent variables $\mathbf{x}_{1:T}$, and
- backward $\pi_{0:T}^-(\mathbf{x}_{0:T} | \mathbf{y}, \theta)$ for the image of interest \mathbf{x}_0 .

This idea is justified by the fact that the two joint priors $\pi_{0:T}^+(\mathbf{x}_{0:T})$ and $\pi_{0:T}^-(\mathbf{x}_{0:T})$ are similar thanks to the learning stage. So, we consider here that they are identical, then the convergence is considered as guaranteed. Overall, the entire algorithm is both simple and efficient for three reasons.

- 1) First, it requires the sampling of Gaussians only.
- 2) Second, all the covariances are diagonal be it in the Fourier domain ($t = 0$) or in the spatial one ($t \neq 0$).
- 3) In addition, means and variances are easy to compute, by FFT ($t = 0$) or linear combination ($t \neq 0$).

The main technical details are reported in Appendix and the full details are [1].

B. Noise parameter scale γ_e

Up to a factor, the conditional posterior for γ_e reads

$$\begin{aligned} & \gamma_e^{P/2} \exp \left[-\frac{\gamma_e}{2} \|\bar{\mathbf{y}} - \mathbf{H}_\iota \mathbf{x}\|^2 \right] \gamma_e^{a_0-1} \exp[-b_0 \gamma_e] \mathbb{1}_{+}(\gamma_e) \\ &= \gamma_e^{a_0+P/2-1} \exp \left[-\gamma_e \left(b_0 + \frac{1}{2} \|\bar{\mathbf{y}} - \mathbf{H}_\iota \mathbf{x}\|^2 \right) \right] \mathbb{1}_{+}(\gamma_e) \end{aligned}$$

The advantage of a conjugacy becomes apparent at this point: the conditional posterior for γ_e is in the same family as the prior, namely a Gamma pdf with parameters:

$$\begin{cases} a &= a_0 + P/2 \\ b &= b_0 + \|\bar{\mathbf{y}} - \mathbf{H}_\iota \mathbf{x}\|^2 / 2 \end{cases}$$

the sampling is then direct and efficient.

C. Noise parameter offset m_e

The conditional posterior for m_e clearly appears as:

$$\begin{aligned} & \exp \left[-\frac{\gamma_e}{2} \|(\mathbf{y} - m_e) - \mathbf{H}_\iota \mathbf{x}\|^2 \right] \exp[-p_0 (m_e - m_0)^2 / 2] \\ &= \exp \left[-\frac{p}{2} (m_e - m)^2 \right] \end{aligned}$$

up to a factor, that is a Gauss pdf with precision and mean

$$\begin{cases} p &= p_0 + P \gamma_e \\ m &= p^{-1} (p_0 m_0 + \gamma_e \mathbf{1}^t (\mathbf{y} - \mathbf{H}_\iota \mathbf{x})) \end{cases}$$

and the sampling is also direct and efficient. At this point also, the advantage of a conjugacy is apparent (the prior and the conditional posterior are in the same family).

D. Instrument parameter

The conditional posterior for the instrument parameter ι is also proportional to the joint posterior (10):

$$\exp \left[-\frac{\gamma_e}{2} \|\bar{\mathbf{y}} - \mathbf{H}_\iota \mathbf{x}\|^2 \right] \mathcal{U}(\iota)$$

This pdf is not an usual one and cannot be directly sampled. Among existing sampling algorithms [20], [21], [23], we resort to a Metropolis-Hasting step. Within this family of algorithms, several options are available (independent, random-walk, ...). Here it is efficient to make use of random-walk Metropolis-Hasting with a Gauss excursion.

IV. NUMERICAL ASSESSMENT

A. Simulation details

In order to demonstrate the feasibility and interest of the proposed Hyper-G-DPS, this Section proposes an experimental study. It relies on a toy problem based on the MNIST example set. The method has been implemented¹ and the information regarding the architecture and learning stage are given in [24]. The ground-truth \mathbf{x}^* is a sample of the learned prior (size 32×32 , gray level roughly in $[0, 1]$). The PSF is a Lorentz shape with width parameter $\iota^* = 0.9$ and regarding the noise $\sigma_e^* = 0.05$ and $m_e = 0.1$. The ground-truth \mathbf{x}^* and the measurement (blurred and noisy image) \mathbf{y} , are shown in Fig. 4 (left and middle). Here are some implementation details.

- Regarding the scan order, the algorithm repeats this pattern: update observation parameters v_e and m_e , then ι , followed by the images for $t = 0$ up to $t = T$.
- The image \mathbf{x}_0 is initialized to \mathbf{y} . The $\mathbf{x}_{1:T}$ are set to successive noisy versions through the forward model. The

¹within the computing environment Matlab on a standard PC with a 3.8 GHz CPU and 32 GB of RAM, and a standard GPU...

width ι and the error mean m_e are initialized at random under their prior. Given the scan order and the Gibbs structure, there is no need to initialize v_e .

- As the iterations proceed, the empirical average of the images is updated. The algorithm stops when the difference between successive updates is smaller than a threshold.

Remark — The algorithm has been run numerous times under identical and different scenarios, including variations in ground truth, noise level, PSF and initialisations. It has consistently exhibited both qualitative and quantitative behaviour.

B. Results

Fig. 2 shows a typical result regarding the three unknown parameters. The chains exhibit standard behaviour: the distributions quickly stabilise and appear stationary after about only 250 iterations (burn-in period). From a qualitative view, Fig. 2 shows that the estimated values are nearby the true values (known in this simulation study). The quantitative results are reported in Tab. I.

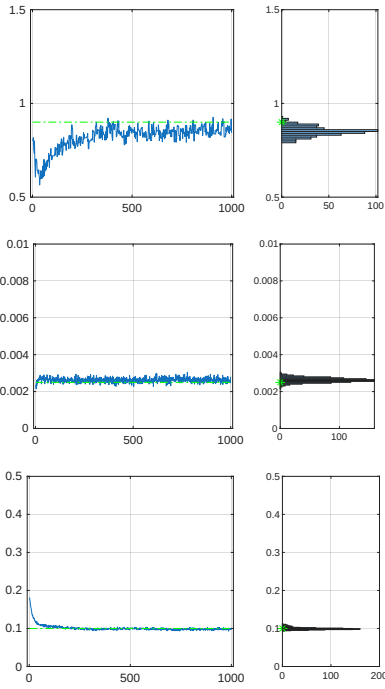


Fig. 2. Samples provided by the Gibbs algorithm for three unknown parameters, from top to bottom: ι , m_e and v_e . They are shown as a function of iteration index (left) and as histograms (right). They are samples of one dimensional marginal pdfs.. The green lines/dots give the true value. Quantitative results are given in Tab. I.

The proposed strategy provides optimal estimations for the unknowns (e.g., Posterior Mean as the MMSE) and coherent tools for uncertainty quantification based on posterior standard deviations (PSD). For each parameter, it is clear from Tab. I that the true value lies within the interval centered on the estimate and of width two standard deviations.

Finally, Fig. 4-right yield the estimated image. The blur and the noise are significantly reduced in the resulting image (Fig. 4-right) with respect to the measurement (Fig. 4-middle)

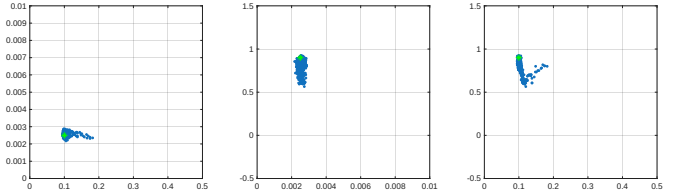


Fig. 3. Point clouds for two dimensional marginals pdfs for three unknown parameters: ι , m_e and v_e . From left to right: (m_e, v_e) , (v_e, ι) , and (m_e, ι) . The sample are given in blue and the true value is given in green. See also Fig. 2 for one dimensional plots and Tab. I for quantitative assessment.

	ι	m_e	v_e
True	0.90	0.1	0.00250
Estimate	0.82	0.103	0.00254
Error	8.9%	3.29%	1.4%
PSD	0.063	0.0082	0.000116
$\pm 2\text{PSD}$	✓	✓	✓

TABLE I

Results for the three unknown parameters ι , m_e and v_e : true and estimated values (first and second row) then the error (third row). The Posterior Standard Deviation (PSD) is then given and the ✓ indicates that the true value does lie within the interval centered on the estimate and of width two PSD. See also Figs. 2 and 3.

and it closely matches the original image (Fig. 4-left). This result is confirmed by the cross-sections also shown in Fig. 4. From Fig. 5 it is clear that, for each pixel, the true value also lies within the interval centered on the estimate and of width two standard deviations.

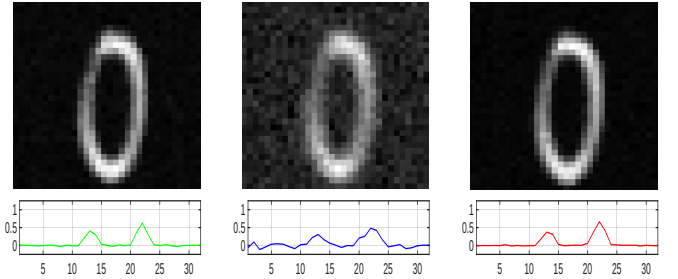


Fig. 4. Left to right: true image \mathbf{x}^* , measurements \mathbf{y} and estimated image $\hat{\mathbf{x}}$. The figure shows the images themselves (top) and cross-sections (bottom).

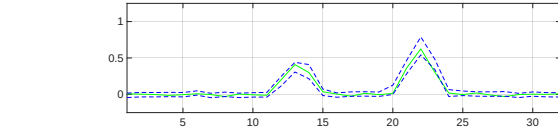


Fig. 5. Cross-sections of \mathbf{x}^* (plain green) and the “uncertainty” intervals (dashed blue) centered on the estimate and of width two standard deviations.

C. Efficiency, computation time and some comments

The algorithm produces N samples of the images and the parameters, $\mathbf{x}_{0:T}^{(n)}$ and $\boldsymbol{\theta}^{(n)}$ for $n = 1, \dots, N$ under the joint posterior pdf for $\mathbf{x}_{0:T}$ and $\boldsymbol{\theta}$. Note that each iteration n involves updating the three parameters $\boldsymbol{\theta} = [\iota, m_e, v_e]$ and all the images \mathbf{x}_t (for $t = 0, \dots, T$).

As mentioned earlier, as the iterations progress, the empirical average of the images $\mathbf{x}_0^{(n)}$ (which approximates the posterior mean) is updated. The iterations stop when the difference between successive updates becomes smaller than a threshold, here set to 10^{-2} . The algorithm thus iterated $N = 1012$ times taking 62 seconds. Most of the calculation time (about 80%) is due to the passage through the network.

A particular feature of the Hyper-G-PDF sampling scheme, inherited from G-DPS, is that, ultimately, each iteration n requires only a single pass through the neural network (to update $\mathbf{x}_0^{(n)}$). Therefore, scaling up to larger images does not appear to be an obstacle.

Another major practical advantage of Hyper-G-DSP, also inherited from G-DPS, is that it does not require the adjustment of any algorithm parameters or fine-tuning quantities, unlike many other algorithms (apart from the number of iterations).

V. CONCLUSION

This paper deals with numerical methods for solving inverse problems when the observation model is linear with additive Gauss noise. The focus is on the delicate issue of estimating multiple parameters of the observation system: width of the point spread function and also mean and variance of noise/error. This is a crucial feature of the proposed method to estimate them in addition to the image of interest. The developments are within a Bayesian framework providing optimal estimates and uncertainty quantification. This issue has already been addressed in the literature and several solutions have been proposed, but not really in cases where the prior for the image is defined on the basis of a diffusion model. In the latter case, our recent contribution [1] allows for proper handling of conditional distributions for images, thereby enabling the inclusion of the conditional posterior for parameters and posterior given these parameters.

More precisely, we use a Gibbs loop which splits the overall problem in far simpler sub-problems: iteratively sample each parameter and each image under its conditional posterior.

The simulation study focuses on parameter estimation issue and it is based on the MNIST example set. The proposed method provides accurate and coherent elements for uncertainty quantification, as well as accurate parameters estimation and image restoration. The numerical study also confirms the remarkable computational efficiency.

Conclusively, the proposed paper addresses the crucial question of estimating instrument and noise parameters, in addition to the unknown image, in inverse problem based on a diffusion prior. It provides a novel, accurate and efficient solution.

To go further, it would be interesting to address model selection [25], [26], especially selection of a model for instrument an/or noise from a given list.

APPENDIX

This appendix provides computational details concerning the Gibbs algorithm used to sample the extended image $\mathbf{x}_{0:T}$. Our previous paper [1] is devoted to this algorithm and gives more details. It samples each \mathbf{x}_t in turn under its conditional

pdf $\pi_{t|*}(\mathbf{x}_t | \mathbf{y}, \boldsymbol{\theta}, \mathbf{x}_{t|*})$ where $(t|*)$ is the set of times from 0 to T except t itself. The structure of these conditional pdfs is based on the hierarchical model presented in Fig. 1.

1 - *Image of interest* — Regarding \mathbf{x}_0 , it is sampled under

$$\begin{aligned} \pi_{0|*}(\mathbf{x}_0 | \mathbf{y}, \boldsymbol{\theta}, \mathbf{x}_{0|*}) &\propto p_{0|1}^-(\mathbf{x}_0 | \mathbf{x}_1) f(\mathbf{y} | \mathbf{x}_0, \boldsymbol{\theta}) \\ &= \mathcal{N}(\mathbf{x}_0; \boldsymbol{\mu}_0(\mathbf{x}_1), v_0^- \mathbf{I}) \mathcal{N}(\mathbf{y}; m_e + \mathbf{H}\mathbf{x}_0, v_e \mathbf{I}) \end{aligned}$$

which reveals a linear-Gauss problem and the Wiener/Tikhonov solution. So, the conditional posterior is Gauss with precision and expectation.

$$\begin{cases} \boldsymbol{\Gamma}_0 &= \mathbf{H}_t^t \mathbf{H}_t / v_e + \mathbf{I} / v_0^- \\ \boldsymbol{\varepsilon}_0 &= \boldsymbol{\Gamma}_0^{-1} [\mathbf{H}_t^t (\mathbf{y} - m_e) / v_e + \boldsymbol{\mu}_0(\mathbf{x}_1) / v_0^-] \end{cases}$$

Sampling is particularly effective in the Fourier plane: the components are independent and Gaussian, and their mean and variance are easily obtained by simple FFT [8].

2.1 - *Latent images* ($t \neq T$) — The \mathbf{x}_t are sampled under

$$\begin{aligned} \pi_{t|*}(\mathbf{x}_t | \mathbf{y}, \mathbf{x}_{t|*}) &\propto p_{t|t-1}^+(\mathbf{x}_t | \mathbf{x}_{t-1}) p_{t+1|t}^+(\mathbf{x}_{t+1} | \mathbf{x}_t) \\ &= \mathcal{N}(\mathbf{x}_t; k_t \mathbf{x}_{t-1}, v_t^+ \mathbf{I}) \mathcal{N}(\mathbf{x}_{t+1}; k_{t+1} \mathbf{x}_t, v_{t+1}^+ \mathbf{I}) \end{aligned}$$

also yields a Gauss pdf with precision $\gamma_t \mathbf{I}$ and expectation $\boldsymbol{\varepsilon}_t$

$$\begin{cases} \gamma_t &= 1/v_t^+ + k_{t+1}^2/v_{t+1}^+ \\ \boldsymbol{\varepsilon}_t &= \gamma_t^{-1} (k_t \mathbf{x}_{t-1} / v_t^+ + k_{t+1} \mathbf{x}_{t+1} / v_{t+1}^+) \end{cases}$$

2.2 - *Latent image* ($t = T$) — For the case of \mathbf{x}_T

$$\begin{aligned} \pi_{T|*}(\mathbf{x}_T | \mathbf{y}, \mathbf{x}_{T|*}) &= p_{T|T-1}^+(\mathbf{x}_T | \mathbf{x}_{T-1}) \\ &= \mathcal{N}(\mathbf{x}_T; k_T \mathbf{x}_{T-1}, v_T^+ \mathbf{I}) \end{aligned}$$

i.e., simply the last step in the forward process: a Gaussian with precision $\gamma_T \mathbf{I}$ and expectation $\boldsymbol{\varepsilon}_T$

$$\begin{cases} \gamma_T &= 1/v_T^+ \\ \boldsymbol{\varepsilon}_T &= k_T \mathbf{x}_{T-1} \end{cases}$$

ACKNOWLEDGMENT

The author warmly thanks Liam Moroy, Guillaume Bourmaud, Frédéric Champagnat, Marcelo Pereyra and Charlesquin Kemajou for their help.

This work is conducted within project *PEPR Origins*, reference ANR-22-EXOR-0016, supported by the France 2030 plan managed by Agence Nationale de la Recherche. It also received financial support from the French government in the framework of the University of Bordeaux's France 2030 program / RRI ORIGINS.

REFERENCES

- [1] J.-F. Giovannelli, “A Gibbs posterior sampler for inverse problem based on prior diffusion model,” *submitted to EUSIPCO, European Signal Processing Conference*, Aug. 2026.
- [2] P. C. Hansen, *Discrete Inverse Problems: Insight and Algorithms*. Philadelphia, USA: Society for Industrial and Applied Mathematics, 2010.
- [3] J. Kaipio and E. Somersalo, *Statistical and computational inverse problems*. Berlin, Germany: Springer, 2005.
- [4] J. C. Santamarina and D. Fratta, *Discrete Signals and Inverse Problems: An Introduction for Engineers and Scientists*. Chichester, England: WileyBlackwell, 2005.
- [5] C. R. Vogel, *Computational Methods for Inverse Problems*, ser. Frontiers in Applied Mathematics. SIAM, 2002, vol. 23.
- [6] M. Pereyra, N. Dobigeon, H. Batatia, and J.-Y. Tourneret, “Estimating the granularity coefficient of a Potts-Markov random field within a Markov Chain Monte Carlo algorithm,” *IEEE Trans. Image Processing*, vol. 22, no. 6, pp. 2385–2397, 2013.
- [7] F. Orieux, J.-F. Giovannelli, T. Rodet, H. Ayasso, M. Husson, and A. Abergel, “Super-resolution in map-making based on a physical instrument model and regularized inversion. Application to SPIRE/Herschel,” *Astron. Astrophys.*, vol. 539, Mar. 2012.
- [8] F. Orieux, J.-F. Giovannelli, and T. Rodet, “Bayesian estimation of regularization and point spread function parameters for Wiener–Hunt deconvolution,” *J. Opt. Soc. Amer.*, vol. 27, no. 7, pp. 1593–1607, July 2010.
- [9] N. Dobigeon, A. Hero, and J.-Y. Tourneret, “Hierarchical Bayesian sparse image reconstruction with application to MRFM,” *IEEE Trans. Image Processing*, vol. 18, no. 9, Sep. 2009.
- [10] T. Bishop, R. Molina, and J. Hopgood, “Blind restoration of blurred photographs via AR modelling and MCMC,” in *Proc. IEEE ICIP*, Oct. 2008.
- [11] P. Campisi and E. K., Eds., *Blind Image Deconvolution*. CRC Press, 2007.
- [12] L. Mugnier, T. Fusco, and J.-M. Conan, “MISTRAL: a myopic edge-preserving image restoration method, with application to astronomical adaptive-optics-corrected long-exposure images,” *J. Opt. Soc. Amer.*, vol. 21, no. 10, pp. 1841–1854, Oct. 2004.
- [13] S. H. Chan, *Tutorial on Diffusion Models for Imaging and Vision*, ser. Foundations and Trends in Machine Learning. Hanover, MA, USA: Now Publishers Inc, Jan. 2024.
- [14] F. D. S. Ribeiro and B. Glocker, *Demystifying Variational Diffusion Models*, ser. Foundations and Trends in Machine Learning. Hanover, MA, USA: Now Publishers Inc, Jan. 2025.
- [15] P. Nakkiran, A. Bradley, and M. Zhou, Hattieand Advani, *Step-by-Step Diffusion: An Elementary Tutorial*, ser. Foundations and Trends in Machine Learning. Hanover, MA, USA: Now Publishers Inc, 2025.
- [16] H. Chung, J. Kim, M. T. Mccann, M. L. Klasky, and J. C. Ye, “Diffusion posterior sampling for general noisy inverse problems,” 2024.
- [17] J. Song, A. Vahdat, M. Mardani, and J. Kautz, “Pseudoinverse-guided diffusion models for inverse problems,” in *International Conference on Learning Representations*, 2023.
- [18] A. Yan, L. Mugnier, J.-F. Giovannelli, R. Fétick, and C. Petit, “Marginalized myopic deconvolution of adaptive optics corrected images using MCMC methods,” *Journal of Astronomical Telescopes Instruments and Systems*, vol. 9, no. 4, Nov. 2023.
- [19] R. J.-L. Fétick, L. M. Mugnier, T. Fusco, and B. Neichel, “Blind deconvolution in astronomy with adaptive optics: the parametric marginal approach,” *Monthly Notices of the Royal Astronomical Society*, vol. 496, no. 4, pp. 4209–4220, Aug. 2020.
- [20] C. P. Robert, *The Bayesian Choice. From decision-theoretic foundations to computational implementation*, ser. Springer Texts in Statistics. New York, USA: Springer Verlag, 2007.
- [21] S. Brooks, A. Gelman, G. L. Jones, and X.-L. Meng, *Handbook of Markov Chain Monte Carlo*. Boca Raton, USA: Chapman & Hall / CRC, 2011.
- [22] N. Yismaw, U. S. Kamilov, and M. S. Asif, “Gaussian is all you need: A unified framework for solving inverse problems via diffusion posterior sampling,” *IEEE Trans. Computational Imaging*, vol. 11, pp. 1020–1030, 2025.
- [23] M. Girolami and B. Calderhead, “Riemannian manifold Hamiltonian Monte Carlo (with discussion),” *J. R. Statist. Soc. B*, vol. 73, pp. 123–214, 2011.
- [24] MatlabDoc (fr.mathworks.com/help/), “Generate images using diffusion,” *deeplearning/ug/generate-images-using-diffusion.html*, 2023.
- [25] T. Ando, *Bayesian model selection and statistical modeling*. Boca Raton, USA: Chapman & Hall/CRC, 2010.
- [26] J. Ding, V. Tarokh, and Y. Yang, “Model selection techniques: An overview,” *IEEE Signal Proc. Mag.*, vol. 35, no. 6, pp. 16–34, Nov. 2018.